Spectroscopic characterization of Er^{3+} transitions in $Bi_4Si_3O_{12}$

2004 J. Phys.: Condens. Matter 16 5925

(http://iopscience.iop.org/0953-8984/16/32/025)

INSTITUTE OF PHYSICS PUBLISHING JOURNAL OF PHYSICS: CONDENSED MATTER

J. Phys.: Condens. Matter **16** (2004) 5925–5936 PII: S0953-8984(04)79102-X

Spectroscopic characterization of Er^{3+} transitions in $Bi_4Si_3O_{12}$

A Lira C[1], I Camarillo[1], E Camarillo[2], F Ramos[1], M Flores[1] and U Caldiño[1]

[1] Departamento de Física, Universidad Autónoma Metropolitana-Iztapalapa, PO Box 55-534, 09340 México, DF, Mexico
[2] Instituto de Física, Universidad Nacional Autónoma de México, PO Box 20-364, 01000 México, DF, Mexico

E-mail: cald@xanum.uam.mx

Received 7 April 2004
Published 30 July 2004
Online at stacks.iop.org/JPhysCM/16/5925
doi:10.1088/0953-8984/16/32/025

Abstract

A systematic investigation of optical absorption and luminescence is presented for Er^{3+} ions in the $Bi_4Si_3O_{12}$ crystal. The intrinsic emission of this crystal gives rise to a radiative energy transfer among the host lattice and Er^{3+} ions. Measured oscillator strengths for seven different transitions from the ground state to excited state manifolds compare favourably with the electric dipole oscillator strengths calculated from the Judd–Ofelt formalism. Radiative lifetimes of the former seven excited states were determined from calculated spontaneous emission probabilities. The ratio of the $^4I_{11/2} \rightarrow {}^4F_{7/2}$ excited state absorption oscillator strength to the $^4I_{15/2} \rightarrow {}^4I_{11/2}$ ground state absorption oscillator strength turned out to be similar to those found for materials pumped efficiently at $^4I_{11/2}$ level excitation wavelengths. The stimulated emission cross section and gain spectra were determined for the $^4I_{13/2} \rightarrow {}^4I_{15/2}$ transition of special interest for laser application.

1. Introduction

Diode pumping solid state lasers have become of great relevance for several technological applications, such as in laser printers, fibre lasers, high brightness displays, optical sensing and optical communications. Er^{3+} is a well known laser ion with transitions in the infrared region around 1550 nm ($^4I_{13/2} \rightarrow {}^4I_{15/2}$) and 3000 nm ($^4I_{11/2} \rightarrow {}^4I_{13/2}$), as well as in the green region around 550 nm ($^4S_{3/2} \rightarrow {}^4I_{15/2}$). Thus, crystals doped with Er^{3+} ions can be excellent for diode pumping lasers because such ions present absorption peaks at around 800 and 980 nm [1–3], which are suitable for excitation with most commercial laser diodes. Moreover, amplification measurements in Er doped fibres have demonstrated that the best

performance in laser gain is achieved pumping at 980 nm [4], which allows the fabrication of compact WDMs for independent routing of the pump and signal light on the same chip, as has been shown for an erbium doped silica based waveguide amplifier integrated with a 980/1530 nm WDM coupler [5]. Er^{3+} ions also exhibit exceptional suitability for optical amplifiers in long distance and high bit rate optical communications, as well as an efficient up-conversion of infrared to visible radiation, which could be useful in a number of potential applications [6, 7]. Such an up-conversion process, on the other hand, can lead to important losses when considering laser gain in the infrared region [8, 9]. In particular, Er^{3+} doped $Bi_4Si_3O_{12}$ (BSO:Er) can become attractive for laser applications, since the bismuth silicate possesses favourable photoconductive, electro-optical and piezoelectric properties for laser light control [10], high isotropic optical activity [10] and a much faster photorefractive response than any other known optical material [11].

In this paper we present a systematic investigation of luminescence and optical absorption spectra of Er^{3+} in BSO in order to identify most of its Stark energy levels, as well as determine the forced electric dipole (ed) transition probabilities and radiative lifetimes of the former excited levels applying the Judd–Ofelt (JO) theory. In this theory the transition probabilities are expressed as the sum of three phenomenological parameters, which can be used to calculate the excited state absorption oscillator strength for transitions from the $^4I_{11/2}$ metastable level to the $^4F_{7/2}$ level in order to obtain some information on the pump efficiency of Er^{3+} ions excited up to their $^4I_{11/2}$ level. The radiative lifetime determined for the $^4I_{13/2}$ metastable level allowed us to obtain the spectral dependence of the stimulated emission cross section and gain for the $^4I_{13/2} \rightarrow {}^4I_{15/2}$ emission of special interest for laser application. The results obtained for BSO:Er are compared with those published for some other Er^{3+} doped materials.

2. Experimental details

A single BSO:Er crystal was grown from stoichiometric melt by the Czochralski technique using platinum crucibles. An oriented seed in the ⟨100⟩ direction was used to obtain a single crystal with good optical quality. However, it was not possible to obtain the specific orientation of the crystal and, hence, only unpolarized measurements were carried out. Bi_2O_3 and SiO_2 were used as starting materials in a 2:3 proportion. The dopant was placed in the melt in the form of Er_2O_3. For the experiments an optically homogeneous $5 \times 4 \times 2.3$ mm^3 prism was cut and polished to optical quality. The erbium concentration (with respect to bismuth) added to the melt was around 5%.

Absorption spectra were recorded on a Varian model Cary 5 spectrophotometer. Fluorescence spectra in the 390–750 nm region were obtained with a Perkin-Elmer LS-50B luminescence spectrometer. Emission spectra in the 750–1050 and 1450–1600 nm spectral regions were acquired by exciting the sample with a Nd:YAG laser (Spectra Physics Quanta Ray) and a Ti–sapphire laser (Coherent), respectively. Emission from the crystal was dispersed by a 0.5 m focal length monochromator and detected by a cooled Hamamatsu photomultiplier tube, for the 750–900 nm region, and a cooled Ge detector, for the IR regions (900–1050 and 1450–1600 nm). A lock-in amplifier (PAR EG&G model 5209) was used to improve the signal to noise ratio. The low temperature emission spectrum in the 1450–1600 nm region was recorded using an Air Products DE-202 cryogenic refrigerator.

3. Results and discussion

3.1. Absorption

Figure 1 shows the room temperature (RT) absorption spectrum in the 320–1600 nm spectral region of Er^{3+} in BSO:Er. It consists of a number of groups of lines corresponding to transitions

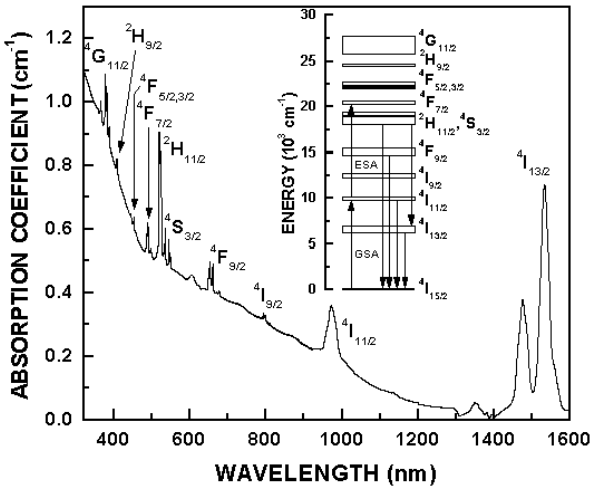

Figure 1. The RT absorption spectrum of Er^{3+} in BSO:Er. The inset shows an approximated scheme of Stark energy levels (associated with the absorption lines) and the ESA mechanism at 975 nm.

between the ground state $^4I_{15/2}$ and higher energy states inside the $4f^{11}$ electronic configuration of the Er^{3+} ion. The ed transitions require different parity states and hence ones between $4f^{11}$ states are forbidden. However, forced ed transitions take place due to opposite parity state admixing from a higher configuration ($4f^{10}5d$) into the same $4f^{11}$ configuration through the electrostatic ligand field odd terms in the coupled state approximation. The absorption spectrum is dominated by the transitions to the multiplets $^2H_{11/2}$ (in accordance with its hypersensitive character) and $^4I_{13/2}$. One can also observe additional lines attributed to a full crystal field splitting of the $^4I_{15/2}$ ground state. All the Er^{3+} transitions, with just the exception of the $^4I_{15/2} \rightarrow {}^4I_{13/2}$ absorption, appear superimposed on broad bands (the crystal absorption edge), which are probably due to several kinds of defect centres. The nature of such bands has not been studied yet. A systematical study of these defects is required in order to improve the technique of growth of BSO crystals. However, this is not the goal of the present work.

The inset of figure 1 displays an approximated scheme of energy levels up to 28 000 cm^{-1} for Er^{3+} in BSO, obtained from the absorption spectrum (figure 1). The global splitting of the ground state was determined from the $^4I_{13/2} \rightarrow {}^4I_{15/2}$ emission spectrum recorded at 20 K. At higher energies the crystal absorption edge becomes so dominant that no more states can be accessed. In fact, the transitions to the multiplets $^4F_{5/2}$, $^4F_{3/2}$, $^2H_{11/2}$ and $^4G_{11/2}$ appear partially darkened by the absorption edge.

3.2. Luminescence

Figure 2 displays the RT spectra for excitation and emission (in the 390–740 nm spectral region). The emission spectrum obtained under $^4G_{11/2}$ multiplet excitation at 378 nm consists of several line groups associated with transitions from the excited multiplets $^2H_{9/2}$, $^4F_{5/2,3/2}$, $^4F_{7/2}$, $^2H_{11/2}$, $^4S_{3/2}$ and $^4F_{9/2}$ to the ground state $^4I_{15/2}$. It can be noticed that the $^2H_{11/2} \rightarrow {}^4I_{15/2}$ emission takes place in spite of the $^2H_{11/2}$ multiplet de-excitation being expected to be predominantly non-radiative, since it is situated about 568 cm^{-1} above the $^4S_{3/2}$ level.

The RT excitation spectrum when the Er^{3+} $^4S_{3/2} \rightarrow {}^4I_{15/2}$ emission is monitored at 550 nm displays several narrow bands in the 350–540 nm region and a broad band in the 200–300 nm

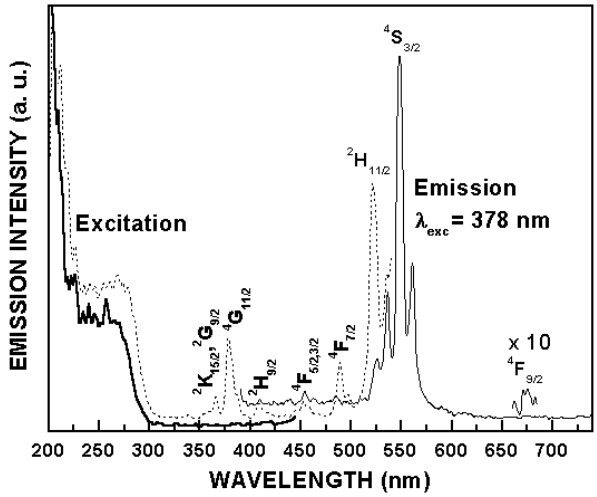

Figure 2. The RT emission spectrum after $^4G_{11/2}$ level excitation at 378 nm and RT excitation spectra monitored in the BSO emission at 505 nm (solid thick curve) and in the Er^{3+} $^4I_{15/2} \rightarrow {}^4S_{3/2}$ emission at 550 nm (dashed curve).

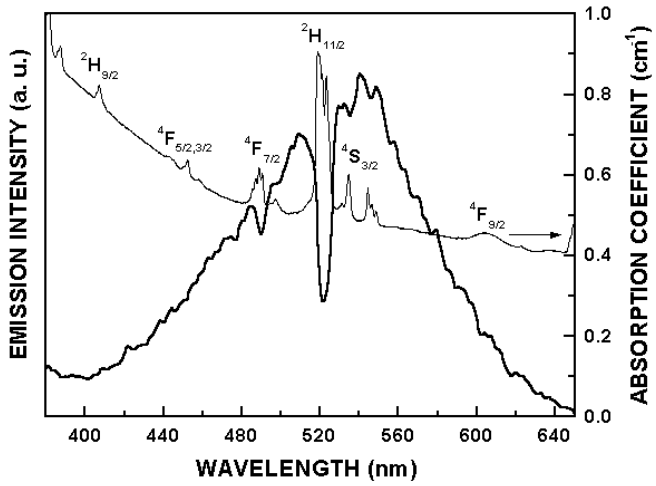

Figure 3. The RT BSO emission spectrum (thick curve) superimposed on the RT BSO:Er^{3+} absorption spectrum (thin curve).

region (figure 2). The narrow bands are associated with Er^{3+} transitions from the ground state to the $^2K_{15/2}$, $^2G_{9/2}$, $^4G_{11/2}$, $^2H_{9/2}$, $^4F_{5/2,3/2}$, $^4F_{7/2}$ and $^2H_{11/2}$ multiplets. The broad band corresponds to the host crystal absorption, since excitation at any wavelength within such a band produces a broad band of emission centred at around 520 nm—that is, the BSO intrinsic emission. In fact, the excitation spectrum corresponding to this emission displays only the broad band assigned to the BSO absorption, as can be appreciated from the excitation spectrum monitored at 505 nm, outside some Er^{3+} emission band (figure 2).

Figure 3 shows the RT emission spectrum of BSO obtained after excitation at 270 nm (within the BSO absorption band). This spectrum has been superimposed on the BSO:Er^{3+}

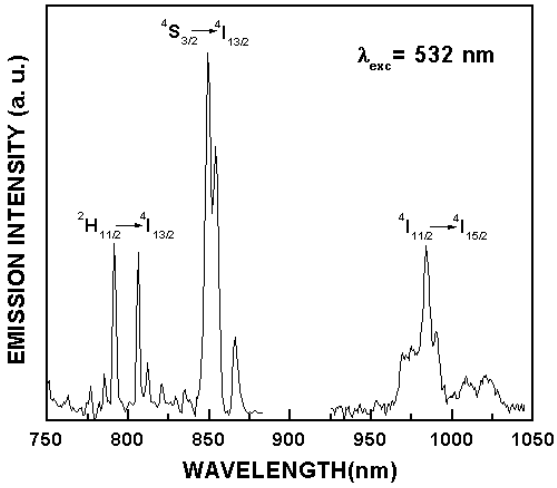

Figure 4. The RT emission spectrum after $^4S_{3/2}$ multiplet excitation at 532 nm.

absorption spectrum in the overlap region in order to facilitate some important observations. Several valleys superimposed on the BSO emission band are quite noticeable, which proves a one-to-one correspondence between the wavelength position of these dips on the absorption peaks associated with the $^4F_{7/2}$, $^2H_{11/2}$ and $^4S_{3/2}$ manifolds. Therefore, it can be inferred that there is a light re-absorption process in the BSO:Er crystal, which can be interpreted, from a microscopic point of view, as a radiative process of energy transfer [12] between resonant energy levels of the host crystal and the Er^{3+} ion.

The RT emission spectrum extending from 750 to 1050 nm is shown in figure 4. This spectrum was obtained by exciting the $^4S_{3/2}$ multiplet at 532 nm. It consists of several emission bands centred at around 799, 853 and 985 nm, which are associated with the transitions $^2H_{11/2} \rightarrow {}^4I_{13/2}$, $^4S_{3/2} \rightarrow {}^4I_{13/2}$ and $^4I_{11/2} \rightarrow {}^4I_{15/2}$, respectively. No emission from the $^4I_{9/2}$ multiplet to the ground state was detected, even after exciting this multiplet at 805 nm. This fact suggests that a predominantly non-radiative relaxation to the $^4I_{11/2}$ emitting state is taking place, in spite of the large energy gap between the multiplets ($\sim$2163 cm^{-1}).

The emission from the $^4I_{13/2}$ multiplet to the $^4I_{15/2}$ ground state of special interest for laser application can be obtained by exciting the level $^4S_{3/2}$ (at 532 nm), $^4I_{9/2}$ (at 805 nm) or $^4I_{11/2}$ (at 975 nm). At this point, it is important to note that the observed radiative energy transfer from the host lattice to Er^{3+} ions does not contribute to this emission, since excitation at any of these wavelengths (532, 805 and 975 nm) is out the host crystal absorption band, 200–300 nm (figure 2). It was also detected that the $^4I_{13/2} \rightarrow {}^4I_{15/2}$ emission is enhanced after exciting the $^4I_{11/2}$ level. Figure 5 displays this emission obtained after 975 nm excitation at RT and 20 K. The low temperature emission spectrum allows one to observe the crystal field splitting of the $^4I_{15/2}$ ground state into its eight Kramers components, which are positioned at 0, 12.8, 40.3, 52.9, 75.9, 86.3, 115.2 and 133.6 cm^{-1}.

3.3. Data analysis

The knowledge of spectroscopic data is required to estimate key laser parameters. Such parameters can be determined from the method based on the JO formalism [13, 14], which has been successfully applied, over the past four decades, to different lanthanide ions in a great

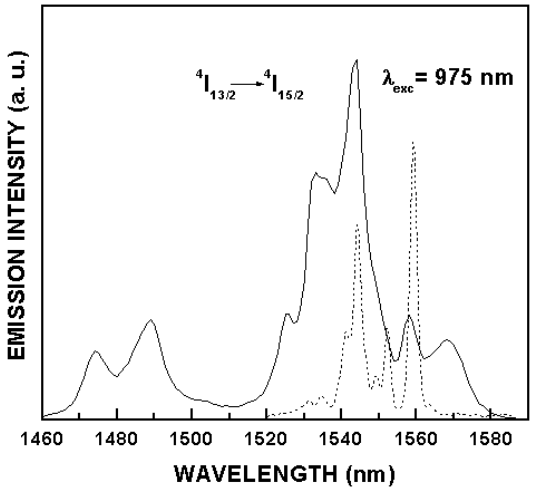

Figure 5. RT and 20 K (dashed curve) emission spectra after $^4I_{11/2}$ multiplet excitation at 975 nm.

variety of isotropic hosts (crystalline and vitreous) [15, 16]. The intra-shell radiative transition probabilities within the ion configuration can be determined through the phenomenological JO parameters. These parameters allow us to calculate the line strength of any radiative transition, as well as radiative lifetimes and fluorescence branching ratios, which are useful quantities for determining stimulated emission cross sections from the emission spectra and the efficiency of lasers and amplifiers.

According to the JO formalism, the line strength for ed transitions between two manifolds defined by their total angular momentum quantum numbers J and J', S_{ed}, in an isotropic material, can be expressed in terms of the Ω_t phenomenological parameters by

$$S_{\mathrm{ed}} = \sum \Omega_t (\langle [L, S]J \| U^t \| [L', S']J' \rangle)^2, \tag{1}$$

where $\langle [L, S]J \| U^t \| [L', S']J' \rangle$ are the doubly reduced matrix elements corresponding to the transition from J to J' levels of the U^t unitary tensor operator of rank t, with $t = 2, 4, 6$, due to the selection rule $|\Delta J| \leqslant 2l$ and $l = 3$ for lanthanide ions. These matrix elements, calculated in the intermediate coupling scheme, were taken from those determined by Carnall [17] for the Er^{3+} ion in LaF_3, since they are almost independent of the environment [18]. Thus, the host dependence in equation (1) is taken into account in the three Ω_2, Ω_4, Ω_6 parameters, which include contributions from the crystal field, the average energy separation of the opposite parity configuration, the interaction between the ion and the immediate environment and the interconfigurational radial integrals. For Er^{3+} ions the $\|U^2\|^2$ matrix element is large for the hypersensitive transitions to the $^2H_{11/2}$ and $^4G_{11/2}$ multiplets, and for the $^4I_{15/2} \rightarrow {}^4I_{13/2}$ transition $\|U^6\|^2$ is very large. A basic assumption involved in equation (1) is that all crystal field levels of the ground state are equally populated, i.e., transitions from all Stark levels of the $^4I_{15/2}$ multiplet are equally probable. The ground state splitting of Er^{3+} in BSO has turned out to be about 134 cm^{-1} and, therefore, this assumption is fulfilled at RT. Moreover, it has been found that the sum of transitions of many different states tends to average out the effects of unequal level populations, as has been observed for crystals with large ground state splitting [19].

On the other hand, the line strength for magnetic dipole (md) transitions between J and J' manifolds is given by

$$S_{\mathrm{md}} = \left(\frac{h}{4\pi mc}\right)^2 (\langle [L, S]J \| \mathbf{L} + 2\mathbf{S} \| [L', S']J' \rangle)^2, \tag{2}$$

where $\mathbf{L} + 2\mathbf{S}$ is the md operator, h is Planck's constant, m is the electron mass and c is the speed of light in vacuum. Considering that the md transitions are parity allowed between states of f^{11} configuration and subject to selection rules $\Delta S = \Delta L = 0$, $\Delta J = 0, \pm 1$ ($0 \leftrightarrow 0$ forbidden) in the Russel–Saunders limit, the host independent matrix elements of $\mathbf{L} + 2\mathbf{S}$ can be calculated from the Carnall expressions [17] given by

$$\langle [L, S]J \| \mathbf{L} + 2\mathbf{S} \| [L, S]J \rangle = \left(\frac{2J+1}{4J(J+1)}\right)^{1/2} [S(S+1) - L(L+1) + 3J(J+1)], \tag{3}$$

$$\langle [L, S]J \| \mathbf{L} + 2\mathbf{S} \| [L, S]J - 1 \rangle = \left\{ \frac{[(S+L+1)^2 - J^2][J^2 - (L-S)^2]}{4J} \right\}^{1/2}, \tag{4}$$

$$\langle [L, S]J \| \mathbf{L} + 2\mathbf{S} \| [L, S]J + 1 \rangle = \left\{ \frac{[(S+L+1)^2 - (J+1)^2][(J+1)^2 - (L-S)^2]}{4(J+1)} \right\}^{1/2}. \tag{5}$$

Thus, the oscillator strength for transitions from an initial J state to a final J' state, including both ed and md contributions, is given by

$$f = \frac{8\pi^2 mc}{3h(2J+1)\bar{\lambda}} (\chi_{\mathrm{ed}} S_{\mathrm{ed}} + \chi_{\mathrm{md}} S_{\mathrm{md}}), \tag{6}$$

where S_{ed} and S_{md} are given by equations (1) and (2), the degeneracy of the level is defined by the $(2J+1)$ factor, $\bar{\lambda}$ is the mean wavelength of the transition between the two manifolds, χ_{ed} and χ_{md} are the local field corrections for the refractivity of the medium which, for an isotropic material of refractive index n (=1.8 for BSO), are usually approximated by

$$\chi_{\mathrm{ed}} = \frac{(n^2+2)^2}{9n} \qquad \text{and} \qquad \chi_{\mathrm{md}} = n. \tag{7}$$

The refractive index was assumed to be constant since its variation over the spectral region analysed is less than 5% [20].

Now, the oscillator strength for transitions from the fundamental J (=15/2) multiplet to the excited J' multiplets can be determined experimentally from the integrated absorption coefficient for each band according to the relation

$$f_{\mathrm{meas}} = \frac{2mc}{\alpha_{\mathrm{f}} h N \bar{\lambda}^2} \int \alpha(\lambda)\, \mathrm{d}\lambda, \tag{8}$$

where α_{f} is the fine structure constant, $\alpha(\lambda)$ is the absorption coefficient (cm^{-1}) at the wavelength λ and N is the concentration of active ions. The absorption coefficient reduces the accuracy of f_{meas} via uncertainties in the integration of the absorption bands, due mainly to noise, and assignment of peaks to each transition. Such uncertainties might be of the order of 5–10%. The value estimated for N (1.26×10^{20} ions cm^{-3}) was taken to be equal to ~13% of the concentration added to the melt, since an actual concentration of 11–15% of that added to the melt has been found in other Er^{3+} doped sillenite oxides [1–3]. Taking into account the uncertainties in the Er^{3+} concentration and the crystal thickness, assumed to be of the order of $\pm 0.25 \times 10^{20}$ ions cm^{-3} and ± 0.04 mm, respectively, the measured oscillator strengths might have a systematic error of the order of 20%.

Table 1. Measured and calculated oscillator strengths. All transitions are from the $^4I_{15/2}$ ground state to the multiplets indicated.

Multiplets	Average wavelength (nm)	$f_{meas} \times 10^{-6}$	$f_{cal} \times 10^{-6}$
$^4I_{13/2}$	1520	1.39 (ed + md) 0.82 (ed), 0.57 (md)	0.82 (ed)
$^4I_{11/2}$	975	0.53	0.35
$^4I_{9/2}$	805	0.22	0.21
$^4F_{9/2}$	656	1.32	1.23
$^4S_{3/2}$	539	0.21	0.33
$^2H_{11/2}$	523	2.00	2.01
$^4F_{7/2}$	490	0.79	1.26

The experimental oscillator strength is due to electron transitions of ed, md and electric quadrupole (eq) character. In most cases, the eq component is of the order of 10^{-10}, which is more than three orders of magnitude smaller than the measured values, and hence eq transitions are negligible for radiative decay. The md component is of the order of 10^{-8} and, therefore, it is unimportant compared with the ed contribution (10^{-6}). However, for the Er^{3+} ion a significant contribution of the md component is involved for the $^4I_{15/2} \rightarrow {}^4I_{13/2}$ absorption transition. Therefore, all the absorption transitions, with the exception of this transition, were assumed to be of ed character. The md contribution to the $^4I_{15/2} \rightarrow {}^4I_{13/2}$ oscillator strength turned out to be 0.57×10^{-6}, which was subtracted from the measured oscillator strength (1.39×10^{-6}) to obtain the purely ed oscillator strength (0.82×10^{-6}).

The JO intensity parameters were, then, estimated from a least squares fitting between the measured (f_{meas}) and calculated (f) oscillator strengths, treating the Ω_t as adjustable parameters. A set of seven equations for transitions from the ground state $^4I_{15/2}$ to multiplets up to $^4F_{7/2}$ were constructed by comparing equation (8) with (6). These transitions do not overlap, and thus they could be analysed separately. The transitions to the higher energy multiplets $^4G_{11/2}$, $^2H_{9/2}$, $^4F_{5/2}$ and $^4F_{3/2}$, which appear partially darkened by the crystal absorption edge, were not taken into account in the fitting because their oscillator strengths could not be evaluated with the same accuracy as those obtained for transitions to the former excited multiplets. The values obtained for the JO parameters are $\Omega_2 = 7.44 \times 10^{-21}$ cm^2, $\Omega_4 = 7.29 \times 10^{-21}$ cm^2 and $\Omega_6 = 6.86 \times 10^{-21}$ cm^2, which follow the trend found for other Er^{3+} doped crystals: $\Omega_2 > \Omega_4 > \Omega_6$ [21–23]. Table 1 displays the calculated and measured oscillator strengths. The quality of our fitting was measured by means of the RMS deviation, which turned out to be equal to 2.6×10^{-7}. Such a deviation is comparable with those obtained for other hosts (1.7×10^{-7} [21], 3.1×10^{-7} [22] and 5.5×10^{-7} [23]). The Er^{3+} $^4I_{15/2} \rightarrow {}^2H_{11/2}$ hypersensitive transition possesses a large $\|U^2\|^2$ matrix element, which has an important influence on the Ω_2 parameter value. It is well known that this parameter is structure sensitive and associated with the asymmetry and covalency of the lanthanide sites [24, 25]. The measured oscillator strength for the $^4I_{15/2} \rightarrow {}^2H_{11/2}$ absorption transition (showed in figure 1) is moderately larger and, therefore, Ω_2 has turned out to be slightly larger than the other two parameters, which might suggest a small structure distortion in the vicinity of Er^{3+} ions.

The JO parameters were used to calculate the total spontaneous emission probabilities, $A(J \rightarrow J')$, for transitions from luminescent multiplets to lower states applying the following relation in terms of the S_{ed} and S_{md} strengths (given by equations (1) and (2)):

$$A(J \rightarrow J') = A_{ed}(J, J') + A_{md}(J, J') = \frac{32\pi^3 c \alpha_f n^2}{3(2J+1)\bar{\lambda}^3}(\chi_{ed} S_{ed} + \chi_{md} S_{md}), \tag{9}$$

where the $(2J + 1)$ degeneracy factor contains implicitly the assumption of equal population of all levels of the initial J multiplet. The $A(J \rightarrow J')$ rate of any level is predominantly due to the forced ed component. However, the $A_{md}(J, J')$ md emission probabilities were also calculated for the transitions $^4I_{13/2} \rightarrow {}^4I_{15/2}$, $^4I_{11/2} \rightarrow {}^4I_{13/2}$, $^4I_{9/2} \rightarrow {}^4I_{11/2}$ and $^4F_{7/2} \rightarrow {}^4F_{9/2}$, which have an important md contribution.

The radiative lifetime for any specific excited state J can, then, be determined from the following relation:

$$\tau_{rad} = \frac{1}{\sum_{J'} A(J \rightarrow J')}, \tag{10}$$

where the sum runs over all final states J'.

The parameter that characterizes the possibility of exciting stimulated emission in a given channel is the intermultiplet luminescence branching ratio $\beta_{J \rightarrow J'}$. The branching ratios can be determined for the $J \rightarrow J'$ transitions from the ratio of the spontaneous radiative emission rate of the observed transition to the total spontaneous emission rate from the initial state:

$$\beta_{J \rightarrow J'} = \frac{A(J \rightarrow J')}{\sum_{J'} A(J \rightarrow J')} = A(J \rightarrow J')\tau_{rad}. \tag{11}$$

The radiative emission probabilities, $A_{ed}(J, J')$ and $A_{md}(J, J')$, the calculated radiative lifetimes and the branching ratios for the main multiplets are listed in table 2. The transitions from the excited multiplets $^4I_{13/2}$, $^4I_{11/2}$, $^4I_{9/2}$, $^4F_{9/2}$, $^4S_{3/2}$, $^2H_{11/2}$ and $^4F_{7/2}$ to the $^4I_{15/2}$ ground state have branching ratios greater than 0.6.

3.4. The $^4I_{13/2} \rightarrow {}^4I_{15/2}$ laser transition

The $^4I_{13/2} \rightarrow {}^4I_{15/2}$ emission of special interest for laser application can be obtained with laser diode excitation up to the $^4I_{9/2}$ or $^4I_{11/2}$ levels. Then, Er^{3+} ions excited decay non-radiatively to the $^4I_{13/2}$ emitting multiplet. The stimulated emission cross section, $\sigma_{em}(\lambda)$, is a key laser parameter for this transition. $\sigma_{em}(\lambda)$ was determined from its emission spectrum, obtained with $^4I_{11/2}$ multiplet excitation at 975 nm, using the Füchtbauer–Ladenburg relation [26]

$$\sigma_{em}(\lambda) = \frac{\lambda^5 \beta_{J \rightarrow J'} I(\lambda)}{8\pi n^2 c \tau_{rad} \int \lambda I(\lambda)\, d\lambda}, \tag{12}$$

where $\beta_{J \rightarrow J'} = 1$, since the initial state $^4I_{13/2}$ is the lowest excited multiplet, τ_{rad} is the purely radiative lifetime of the $^4I_{13/2}$ multiplet. The value calculated for τ_{rad} (=6.91 ms) is within the range of values reported for other Er^{3+} doped crystals, from 2.3 ms [22] to 10.9 ms [20]. Such a radiative lifetime should be comparable with the observed lifetime due to the large energy gap between the $^4I_{13/2}$ and $^4I_{15/2}$ multiplets (6579 cm^{-1}).

Figure 6 displays the gain spectra as a function of the inverted population rate γ, obtained with the relation

$$G(\lambda) = \gamma\sigma_{em}(\lambda) - (1 - \gamma)\sigma_{abs}(\lambda), \tag{13}$$

where $\sigma_{abs}(\lambda) = \alpha/N$ is the absorption cross section. From these spectra it can be observed that lasing should be successful at 1544 nm for a population inversion larger than 50%. At this wavelength the maximum value for the gain is achieved when $\gamma = 1$, for which the stimulated emission cross section turns out to be 11.3×10^{-21} cm^2. This σ_{em} value is of the order of or higher than those reported for other Er^{3+} based laser crystals (9.3×10^{-21} cm^2 for $LaGaO_3$:Er^{3+} [21], 4.5×10^{-21} cm^2 for YAG:Er^{3+} [26] and 3.1×10^{-21} cm^2 for $YAlO_3$:Er^{3+} [26]). However, excitation at the wavelength 975 nm can complicate the pumping of Er^{3+} ions because of a two-step resonant excited state absorption (ESA) from the $^4I_{11/2}$ pump

Table 2. Branching ratios, predicted radiative transition rates of ed and md radiation and calculated radiative lifetimes.

Transition	Average wavelength (nm)	Branching ratio $\beta_{J\to J'}$	Transition rate (s^{-1}) $A_{ed}(J, J')$	Transition rate (s^{-1}) $A_{md}(J, J')$	Calculated radiative lifetime (ms)
$^4I_{13/2} \to {}^4I_{15/2}$	1 532.4	1.00	84.9	59.8	6.91
$^4I_{11/2} \to {}^4I_{15/2}$	985.2	0.77	101.4		7.54
$^4I_{11/2} \to {}^4I_{13/2}$	2 721.8	0.23	14.7	16.5	
$^4I_{9/2} \to {}^4I_{15/2}$	816.3	0.71	104.6		6.80
$^4I_{9/2} \to {}^4I_{13/2}$	1 713.2	0.26	38.9		
$^4I_{9/2} \to {}^4I_{11/2}$	4 622.8	0.03	0.6	3.0	
$^4F_{9/2} \to {}^4I_{15/2}$	679.2	0.90	885.8		1.02
$^4F_{9/2} \to {}^4I_{13/2}$	1 154.9	0.05	45.4		
$^4F_{9/2} \to {}^4I_{11/2}$	2 006.1	0.05	45.6		
$^4F_{9/2} \to {}^4I_{9/2}$	3 544.2	0.00	1.0		
$^4S_{3/2} \to {}^4I_{15/2}$	550.4	0.67	908.0		0.73
$^4S_{3/2} \to {}^4I_{13/2}$	853.0	0.27	374.0		
$^4S_{3/2} \to {}^4I_{11/2}$	1 205.7	0.02	31.8		
$^4S_{3/2} \to {}^4I_{9/2}$	1 631.2	0.04	52.9		
$^4S_{3/2} \to {}^4F_{9/2}$	3 022.1	0.00	0.6		
$^2H_{11/2} \to {}^4I_{15/2}$	529.2	0.93	2032.9		0.46
$^2H_{11/2} \to {}^4I_{13/2}$	799.3	0.03	62.7		
$^2H_{11/2} \to {}^4I_{11/2}$	1 128.5	0.02	35.0		
$^2H_{11/2} \to {}^4I_{9/2}$	1 493.0	0.02	38.3		
$^2H_{11/2} \to {}^4F_{9/2}$	2 579.6	0.00	5.7		
$^2H_{11/2} \to {}^4S_{3/2}$	17 618.6	0.00	0.0		
$^4F_{7/2} \to {}^4I_{15/2}$	489.7	0.79	2266.7		0.35
$^4F_{7/2} \to {}^4I_{13/2}$	723.6	0.12	323.3		
$^4F_{7/2} \to {}^4I_{11/2}$	985.6	0.05	156.0		
$^4F_{7/2} \to {}^4I_{9/2}$	1 252.6	0.03	95.0		
$^4F_{7/2} \to {}^4F_{9/2}$	1 937.4	0.01	3.0	27.0	
$^4F_{7/2} \to {}^4S_{3/2}$	5 397.9	0.00	0.0		
$^4F_{7/2} \to {}^2H_{11/2}$	7 782.1	0.00	0.4		

level to the $^4F_{7/2}$ level, as can be seen in the inset of figure 1. Then, the population of the $^4F_{7/2}$ excited multiplet relaxes non-radiatively to the $^2H_{11/2}$, $^4S_{3/2}$, $^4F_{9/2}$, $^4I_{11/2}$ and $^4I_{13/2}$ emitting states. Thus, we have evaluated the ESA oscillator strength, f_{ESA}, for transitions from the $^4I_{11/2}$ level to the $^4F_{7/2}$ multiplet. The md contribution to such a strength is negligible and, hence, it was determined from equations (1) and (6) using the calculated JO parameters and, for $\bar{\lambda}$, the average energy difference of the levels. The ratio of the $^4I_{11/2} \to {}^4F_{7/2}$ ESA oscillator strength (f_{ESA}) to the $^4I_{15/2} \to {}^4I_{11/2}$ ground state absorption oscillator strength (f_{GSA}) can give some information about the pump efficiency of Er^{3+} ions at 975 nm. This strength ratio has turned out to be about 1.35, which is very similar to the values found for materials pumped efficiently up to the Er^{3+} ion $^4I_{11/2}$ level, such as erbium doped phosphate (1.44) and silicate (1.34) [27, 28]. Moreover, in these materials the very short measured lifetime for the pump level improves the pumping efficiency. Measurements of the $^4I_{11/2}$ level lifetime, as well as some experiments in ESA spectroscopy, can be performed in the future to determine the ESA cross section, which can be used to evaluate suitable pump wavelengths around 975 nm and to predict the saturation pump powers at such wavelengths.

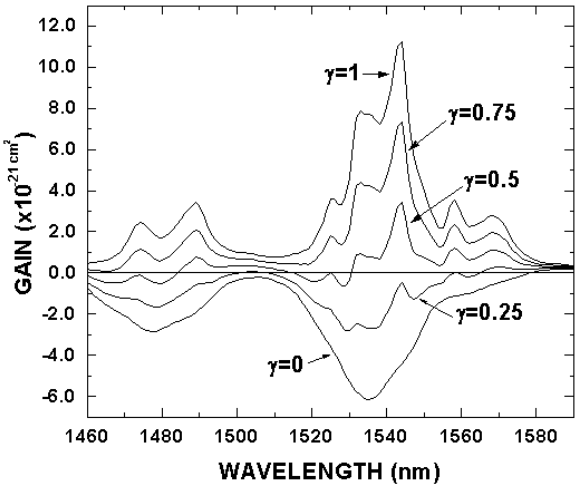

Figure 6. RT gain spectra for the $^4I_{13/2} \leftrightarrow {}^4I_{15/2}$ transition as a function of the inverted population rate γ.

4. Conclusions

A single $Bi_4Si_3O_{12}$ crystal doped with Er^{3+} ions was grown by the Czochralski technique and its optical properties were studied. Experimental results revealed that energy transfer occurs from the host crystal to the Er^{3+} ion via a radiative process. The Judd–Ofelt phenomenological treatment was applied to determine the ed oscillator strengths for transitions from the ground state $^4I_{15/2}$ to the former excited multiplets $^4I_{13/2}$, $^4I_{11/2}$, $^4I_{9/2}$, $^4F_{9/2}$, $^4S_{3/2}$, $^2H_{11/2}$ and $^4F_{7/2}$. These oscillator strengths are in good agreement with those measured within the accuracy limits of such an analysis. The Judd–Ofelt parameters were used to predict the radiative emission rates of the main excited levels. From the gain spectra recorded for the $^4I_{13/2} \rightarrow {}^4I_{15/2}$ emission, of special interest for laser application, it was found that a larger gain is achieved at 1544 wavelength. At this wavelength the stimulated emission cross section, attained with a population inversion of 100%, is of the order of or larger than those reported for other Er^{3+} based laser crystals. The value obtained for the ratio of the $^4I_{11/2} \rightarrow {}^4F_{7/2}$ excited state absorption oscillator strength to the $^4I_{15/2} \rightarrow {}^4I_{11/2}$ ground state absorption oscillator strength turned out to be very similar to the values reported for Er^{3+} doped materials pumped efficiently at $^4I_{11/2}$ level excitation wavelengths.

Acknowledgments

This work was partially supported by the CYTED under subprogramme VIII-12. We are also deeply grateful to Dr José Manuel Hernández (Instituto de Física, UNAM) for most valuable discussions.

References

[1] Lira C A, Caldiño G U, Ramírez M O, Sanz García J A and Bausá L E 2001 *J. Phys.: Condens. Matter* **13** 11067
[2] Ramírez M O, Lira C A, Sanz García J A, Bausá L E and Caldiño G U 2002 *J. Alloys Compounds* **341** 275
[3] Ramírez M O, Bausá L E, Lira C A and Caldiño G U 2002 *J. Mater. Sci. Lett.* **21** 1517

[4] Miniscalco W J 1991 *J. Lightwave Technol.* **9** 234
[5] Hattori K, Kitagawa T, Oguma M, Ohmori Y and Horiguchi M 1994 *Electron. Lett.* **30** 856
[6] Lenth W and Macfarlane R M 1992 *Opt. Photon. News* **3** 8
[7] Downining E, Hesselink L, Ralston J and Macfarlane R 1987 *Science* **273** 1185
[8] Koetke J and Huber G 1995 *Appl. Phys.* B **61** 151
[9] Doualan J L, Le Boulanger P, Girard S, Margerie J, Ermneneux F S and Moncorgé R 1997 *J. Lumin.* **72–74** 179
[10] Solymar L, Webb D J and Grunnet-Jepsen A 1996 *The Physics and Applications of Photorefractive Materials* (Oxford: Clarendon)
[11] Petrov M P, Stepanov S I and Khomenko A V 1991 *Photorefractive Crystals in Coherent Optical Systems* (Berlin: Springer)
[12] Hernández A J, Camarillo E, Loro H and Murrieta S H 2001 *J. Alloys Compounds* **323/324** 714
[13] Judd B R 1962 *Phys. Rev.* **127** 750
[14] Ofelt G S 1962 *J. Chem. Phys.* **37** 511
[15] Henderson B and Imbush G F 1989 *Optical Spectroscopy of Inorganic Solids* ed B Henderson and G F Imbush (Oxford: Clarendon)
[16] Reisfeld R 1987 *Spectroscopy of Solid-State Laser-Type Materials* (*Ettore Majorana International Science Series* vol 30) ed B Di Bartolo (New York: Plenum)
[17] Carnall W T, Fields P R and Wybourne B G 1965 *J. Chem. Phys.* **42** 3797
[18] Riseberg L A and Weber M J 1976 *Progress in Optics* vol 14, ed E Wolf (New York: Elsevier) p 89
[19] Dai H, Stafsudd O M, Dunn B and Momoda L A 1992 *J. Phys. Chem. Solids* **53** 1175
[20] Weber M J 1967 *Phys. Rev.* **157** 262
[21] Sokólska I 2000 *Appl. Phys.* B **71** 157
[22] Amin J, Dussardier B, Schweizer T and Hempstead M 1996 *J. Lumin.* **69** 17
[23] Nuñez L, Lifante G and Cussó F 1996 *Appl. Phys.* B **62** 485
[24] Souza Filho A G, Mendes Filho J, Melo F F A, Custodio M C C, Lebullenger R and Hernandes A C 2000 *J. Phys. Chem. Solids* **61** 1535
[25] Koeppen C, Yamada S, Jiang G, Garito A F and Dalton Larry R 1997 *J. Opt. Soc. Am.* B **14** 155
[26] Payne S A, Chase L L, Smith L-K, Kway L and Krupke W F 1992 *IEEE J. Quantum Electron.* **28** 2619
[27] Quimby R S 1991 *Appl. Opt.* **30** 2546
[28] Quimby R S, Miniscalco W J and Thompson B 1991 Fiber laser sources and amplifiers III *Proc. SPIE* **1581** 72